Journal of Nepal Geological Society, 2000, Vol. 22, pp. 351–358

Electrical resistivity tomography for aquifer imaging

Dipak Raj Pant
Royal Nepal Academy of Science and Technology, G.P.O. Box 3323, Khumaltar, Lalitpur, Nepal

ABSTRACT

Aspects related to the development of a technique called electrical resistance tomography for producing two- or three-dimensional subsurface images of an aquifer have been discussed. The technique is based on the automated measurement and computerised analysis of electrical resistivity changes caused by natural or man-made processes. A subsurface region of the aquifer to be studied is sampled by transmitting electrical energy through it along many paths of known orientations, and the apparent resistivity data derived are used to construct a cross-sectional image of the region of interest.

The physical model experiments and field experiments show that the presented method is effective and flexible for crosshole resistivity imaging of aquifer with bipole-bipole electrode configurations.

INTRODUCTION

The scientific management of water resources has become increasingly important with growing population and technological advances. Groundwater is one of the very important natural resources of the earth. Surface water is the natural parent of groundwater. The magnitude of groundwater reserves is large, but as they are unseen we tend to underestimate them. It is very important that we make use of these underground reserves.

Aquifers are formations that contain sufficient saturated permeable material capable of yielding significant quantities of water. Water has always remained as a natural resource in the aquifer below the ground surface. Water emerges out in the shape of springs, fountains, and flowing wells as a gift of mother nature that has connected valley aquifers with upland mountainous water resources through a confining layer.

Artificial recharge is the intentional redirection of surface water into aquifers. Surplus run-off generated during wet season (monsoon period) which is otherwise lost to flow is recharged underground in order to use it as a water resource during dry period. Storage of surface water in suitable aquifers provides a viable alternative to reservoirs in areas where: land values are high, topographic relief is inadequate, evaporation rates are high, catchment areas are intensively developed, or where toxic algae may compromise the quality of stored water. Based on groundwater quality, transmissivity, current local extraction, and storage capacity, the best receiving aquifers are the recipient of "harvested" stormwater run-off from adjacent housing and wetlands. The water stored during wet season may be recovered in the dry season and used by households for drinking purpose and also for irrigation of gardens and fields throughout the village and urban areas.

In recent years, there has been great interest in developing crosshole DC electrical surveying to image the 2-D and 3-D image of the aquifer. Crosshole resistivity imaging or tomography (Van et al. 1991; Park and Van 1991; Daily and Owen 1991; Shima 1991), in which the source electrode (current injection point) and the potential electrode (measuring point) are placed downhole in two horizontally separated boreholes and moved over a range of depths, is used to reconstruct the conductivity structure of aquifer between the boreholes. In theory, the technique is no more than a geophysical inversion procedure with various array apertures between the boreholes.

This paper describes a flexible and efficient finite element method (FEM) scheme for 2-D resistivity modelling. The 2.5-D Helmholtz equation is used to calculate the 2.5-D Green's function (Zhou et al. 1992; Zhou and Greenhalgh 1997, 1998; Pant et al. 1999) for arbitrary media. The geophysical inversion is accomplished by employing optimisation algorithms (Tarantola 1987).

In this paper the theoretical aspects of forward modelling and inversion are presented. Then the results of physical model experiments and real field experiments to image the aquifers are given.

BASIC THEORY RELATED TO MODELLING AND INVERSION

Forward modelling

Ohm's law relates the current density **J** to the electric field intensity **E** through the conductivity σ, which is a function of the 3-D coordinates $\sigma = \sigma(x,y,z)$.

$$\mathbf{J} = \sigma \mathbf{E}$$

Since stationary electric fields are conservative for the DC resistivity problem,

$$\mathbf{E} = -\nabla U$$

where ∇ is the gradient operator and U is an electric potential function.

Applying the principle of conservation of charge and using the equation of continuity:

$$\nabla.\mathbf{J} = I\,\delta(r-r_c) \qquad r, r_c \in \Omega$$

where I is the injected current specified at a point by the Dirac delta function in an arbitrary closed surface in the studied region Ω.

Above equation can be rewritten as:

$$\nabla.(\sigma\nabla U) = -I\,\delta(r-r_c) \qquad r, r_c \in \Omega \qquad (1)$$

The Green's function G is commonly defined by the potential response to an unit injection I = 1, so the equation becomes

$$\nabla.(\sigma\nabla G) = -I\,\delta(r-r_c) \qquad r, r_c \in \Omega \qquad (2)$$

By Equations (1) and (2), the potential response to current and Green's function is:

$$U(r_c,r_p) = IG(r_c,r_p) \qquad (3)$$

Currently several numerical methods (Zienkiewicz 1971; Dey and Morrison 1979a,b; Queralt and Marcuello 1991; Zhao and Yedlin 1996) may be used to solve the above Equation (1) by finite difference method, (2) by FEM using the Galerkin's solution (also called weighted residual solution), and (3) by FEM using the Variational Principle.

The FEM theory using the Galerkin's solution is selected in this paper. Such a solution can relatively easily handle complicated geometry, general boundary conditions, and variable and non-linear material properties. The technique involves two steps: (1) assumption of general functional behaviour of the dependent field variable to approximately satisfy the given differential equation and boundary conditions and (2) substitution of the approximation into the original differential equation and boundary conditions. This results in some error called a residual, which is made to vanish with a weighting function over the computational range.

Let a defined differential equation be:

$$L\Phi = f, \qquad r \in \Omega \qquad (4)$$

$$\frac{\partial \Phi}{\partial n} + B\Phi = 0, \qquad r \in \partial\Omega$$

where f is known function and Φ is exact solution. Approximation to Φ is expressed as:

$$\Phi(r) = \sum_i N_i(r)\,\Phi_i \qquad (5)$$

where Φ_i coefficients to be determined and $N_i(r)$ are set of chosen shape functions that satisfy the boundary condition.

By Equations (4) and (5), we form the residual:

$$R(r) = L\Phi - f \qquad (6)$$

The weighted residual method seeks the solution Φ in which the weighted average vanishes over the solution domain

$$\int_\Omega W_j(r)\,R(r)\,dr = \int_\Omega W_j(r)\,[L\Phi - f]\,dr = 0, (j = 1,2,3,...m)$$

W_j are chosen as m linearly independent weighting functions.

Galerkin's solution takes the weighting functions to be same as the shape functions $W_j = N_j(r)$ used to represent Φ, so above equation becomes

$$\sum_i \int_\Omega N_j(r)\,[LN_i(r)]\,\Phi_i\,dr = \int_\Omega N_j(r) f\,dr, (j = 1,2,3,...m) \qquad (7)$$

The 2-D or 3-D Helmholtz equation is well-known and is given as:

$$\nabla_{2,3}^2\Phi + k^2(c)\Phi = 0$$

which describes a 2-D line-source or 3-D point-source wavefield Φ when the wavenumber $k = w/c$ is given by a positive constant.

The 2.5-D approximation Helmhotz equation (Takenaka and Kennett 1996 a,b) is:

$$\nabla.[a(x,z)\nabla\Phi] + k_a^2(a(x,z),b(x,z),k_y)\Phi = 0$$

where $\nabla = (\partial_x,\partial_y)$, Φ is the Fourier-cosine transform of Φ and $a(x,z)$ and $b(x,z)$ are arbitrary model functions that represent model properties in the (x,z)-plane.

According to the 2.5-D approximation, the current electrode is assumed to be a point-source, and the conductivity σ model is considered to be 2-D, that is the variation of the conductivity depends upon only the x and z-coordinates (Dey and Morisson 1979a,b; Williamson and Pratt 1995; Cao and Greenhalgh 1997). The source is set a coordinate $(x_c, 0, z_c)$ and the Fourier-cosine transform is taken with respect to the y-coordinate, which transforms Equation (1) into:

$$\nabla.(\sigma\nabla U) - k_y^2\sigma U = -I\,[\delta(x-x_c)\,\delta(z-z_c)]/2 \qquad (8)$$

where $\nabla = (\partial_x, \partial_z)$ and the 2-D gradient in the (x,z)-plane is:

$$U(x, z, k_y) = \int U(x,y,z)\cos(k_y y)\, dy$$

Comparing Equation (8) with 2.5-D approximation Helmholtz equation, we find it is the specified form of the 2.5-D Helmholtz equation. (a=σ(x,z), b=constant, $k_a = -k_y^2\sigma(x,z)$).

Substituting the operator, the source-term and the boundary condition (mixed-boundary condition) of Equation (8) into Equation (7), we get

$$\sum_i \{\int_\Omega [a\nabla N_i \cdot \nabla N_j - k_a^2(a,b,k_y)\, N_i\, N_j]\, dr + \int_{\partial\Omega} a N_j B N_i\, d\Gamma\}\Phi_i = (1/2)\, N_j\, \delta_{is} \quad (j= 1,2,3,...m) \qquad (9)$$

where $\delta_{is} = 1$ if $r_i = r_s$, and $\delta_{is} = 0$ if $r_i \neq r_s$. Γ is boundary element (Earth surface and artificial boundary). After discretisation of the integral range, above equation reduces to system of linear equations, which can be solved with standard algorithm for all the nodal values Φ_i.

Equation (9) reduces to the following for the 2.5-D Green's function in DC resistivity modelling:

$$\sum_i \{\int_\Omega [\sigma\nabla N_i \cdot \nabla N_j + k_y^2 \sigma\, N_i\, N_j]\, dr + \int_{\partial\Omega} \sigma\, N_j\, B N_i d\Gamma\}$$

$$G_i^{2.5D} = N_j d_{is} \quad (j= 1,2,3,..., N) \qquad (10)$$

Here, N_i (i = 1,2,3,..., N) is the i-th shape function in the Galerkin's solution and $G_i^{2.5D}$ (i = 1,2,3,..., N) is the i-th nodal values of the Green's function. N is the total number of shape functions.

To calculate the integrals in Equation (10), computational range Ω and the boundary $\partial\Omega$ is divided into a set of subranges (elements) and segments, so that the equation reduces to the following linear equation system:

$$M\, G^{2.5D} = b_s \qquad (11)$$

where

$$M = (M_{ij})_{N\times N}, \qquad M_{ij} = \sum_e (A_{ij}^e + B_{ij}^e)$$

$$G^{2.5D} = \{G_i^{2.5D}\}^T, \quad (i = 1,2,3,..., N)$$

$$b_s = \{ N_i\, d_{is}\}^T, \qquad (i = 1,2,3,..., N)$$

and

$$A_{ij}^e = \int_\Omega \sigma(r)\, [\nabla N_i(r).\nabla N_j(r) + k_y^2 N_i(r) N_j(r)]\, dr$$

$$B_{ij}^e = \int_\Gamma \sigma(r) N_i(r) B N_j(r)\, d\Gamma$$

The matrix A_{ij}^e is called the inner element matrix and B_{ij}^e is called the boundary element matrix. The matrix M is a diagonally dominant, positive and symmetric matrix (Dey and Morrison 1979a,b). This property of M enables one to apply the banded Cholesky decomposition ($M = LL^T$) in solving Equation (11). Once the element matrices are calculated, one can solve the linear equation system to obtain the Galerkin's solution of the 2.5-D Green's function.

The apparent resistivity is defined as:

$$\rho_a = C \times \Delta U / I$$

where

$\Delta U = U_M - U_N$, potential difference between two potential electrodes M and N;

I = total current entering the ground;

C = geometric factor which depends on the electrode array configuration.

A general form of apparent resistivity for pole-pole, pole-bipole, bipole-pole and bipole-bipole electrode arrays after Zhou and Greenhalgh (1997) is:

$$\rho_a = C\, [\partial G_{MN}^{3D}(r_A) - \partial G_{MN}^{3D}(r_B)] \qquad (12)$$

where

$$\partial G_{MN}^{3D}(r) = \tfrac{1}{2} [F_c^{-1} \times \{G^{2.5D}(r_M, r) - G^{2.5D}(r_N, r)\}]$$

F_c^{-1} is inverse Fourier transform. The expression (12) is for any surface or crosshole surveying configuration. It demonstrates that the apparent resistivities for different arrays can be directly calculated from the Green's functions. It shows that the forward modelling for apparent resistivity involves:

- computation of the Green's functions for the current electrodes in an electrode array and
- calculation of geometric factor.

Inversion

In a practical sense, geophysical data are incomplete due to the limited number of sampling in both space and time. Obsevations are contaminated by various forms of noise and the geophysical inverse problem is ill-posed. Inversion has multiple solutions i.e. there exist many models that produce a satisfactory fit to the observed data.

Inversion problem is formulated as an optimisation scheme to find the model (medium structure) that gives the best fit between the synthetic and observed geophysical data. General well-known solutions are (Menke 1984; Tarantola 1987; Kennett and Willamson 1988; Oldenburg et al. 1993; Scale and Smith 1994; Parker 1994): (1) Tikhonov solution (general iterative solution, iteratively linearised solution, Levernburg-Marquart solution, and conjugate gradient solution); (2) Smoothest model solution (Occam's inversion); and (3) Subset solution.

It is a common practice to use an objective (or misfit) function as a quantitative measure of the fit between the calculated and observed geophysical data. The l_2-norm objective function (Tarantola 1987) for evaluating the goodness of fit in the data-space [$\Phi_d(m)$] and the model-space [$\Phi_m(m)$] is:

$$\Phi_d(m) = || W_d [d_0 - d(m)] ||^2 \quad (13)$$

$$\Phi_m(m) = || W_m (m - m_0) ||^2 \quad (14)$$

where

d_0 = vectors of observed data

$d(m)$ = vectors of computed data and calculated with Finite Element Method when the model;

$m = \{m_1, m_2, ..., m_n\}$ is given;

m, m_0 = are the unknown (to be determined) and initial primary estimated model-parameter vectors;

W_d = weighting matrices of the data set; and

W_m = weighting matrices of the model parameters.

Also used sometimes is the Tikhonov function (Tikhonov and Arsenin 1977) defined in general form as:

$$\Phi(m) = \Phi_d(m) + \lambda \Phi_m(m)$$

where λ is termed a regularisation parameter (also called trade-off or damping parameter).

The aim of inversion is to find the model by solving the optimisation problem:

$$\min \{\Phi(m)\} = \min \{\Phi_d(m) + \lambda \Phi_m(m)\}$$

If $W_d = C^{-1}_d$, $W_m = C^{-1}_m$, $\lambda = 1$ solution is called Generalised Least Squares solution (Tarantola and Valette 1982). Taking different weighting operators λ yields Weighted Least Squares solution (Menke 1984).

Three kinds of mathematical technique are chosen to solve optimisation problem :

(1) Global minimisation search such as genetic algorithm and simulating annealing method (Stoffa and Sen 1991; Chunduru et al. 1995, 1996; Dittmer and Szymansk 1995);

(2) Local minimisation search such as linearised iteration, steepest descent, conjugate gradient and quasi-Newton method (Minoux 1986; Tarantola 1987); and

(3) Hybrid method such as artificial neural networks that combines with linearised inversion (Teles and Carmo 1999).

The first kinds of inversion algorithm are computationally expensive and have been applied only to simple models. The second kinds of inversion algorithm offer advantages for effectiveness and computational efficiency. A good initial guess or prior information (drawn from the integration of geological and geophysical observations) is necessary to avoid local minima. The third kinds of inversion take an advantage of the above two kinds.

METHODOLOGY OF LABORATORY MODELLING AND FIELD OBSERVATIONS

Three-dimensional water tank modelling

The sketch of three-dimensional water tank physical resistivity modelling system is illustrated in Fig. 1. A SYSCAL-R2 digital resistivity instrument was interfaced to a PC and can store 390 set of measurements, each of which includes self-potential, current magnitude, voltage difference, and information on the surveying configuration. The dimension of the water-tank was 60 cm x 60 cm x 90 cm and was made of PVC material.

The tank was filled with ordinary tap water. The top of the tank contained railings (with millimetres marking) to mount the electrodes and record their horizontal and perpendicular motions x and y-coordinates. The markings were made on the electrodes itself to record the vertical motion (z-coordinate). The four electrodes were constructed using stainless steel tube (SST) and enamelled copper wire (ECW). The SST was of length 50 cm, diameter 1.4 mm and wall thickness of 0.2 mm. If the electrode was required to be placed at infinity (pole-pole or pole-bipole configurations) then SST of length 1m was used. The diameter of the ECW was 0.71 mm.

The ECW was inserted inside the SST and pushed further down from the bottom of the SST. The distance between two bottoms (bottom of the SST and the bottom of the ECW) depended upon the separation among two electrodes needed for various experiments (some had 5 cm while others even had 2 cm). The bottom of the SST became one of the

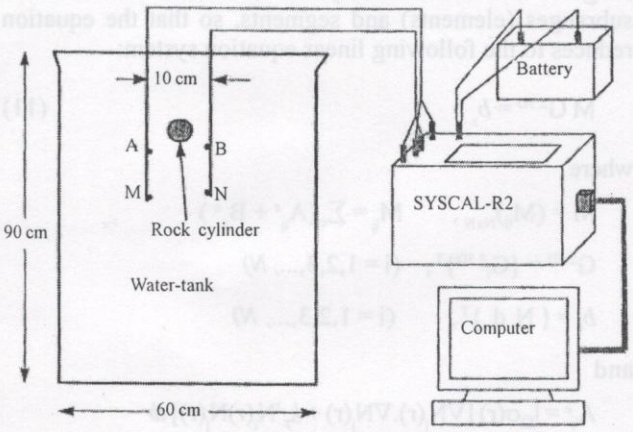

Fig. 1: Physical resistivity modelling experiment used in the imaging experiments. A (source) and B (sink) are current electrodes, M (positive) and N (negative) are potential electrodes. A SYSCAL-R2 digital resistivity instrument stores self-potential, current, voltage, and surveying information, which are then transmitted to the interfaced PC.

electrodes. The bottom tip of the ECW became the other electrode. To insulate the SST from the host material so that it does not act as a line source, heat shrink tubing was used at the outer diameter of the SST. The enamel on the ECW acted as the insulator that separated the copper electrode from the stainless SST.

Normally the SST tip was used as the current electrode (source and/or sink). The ECW tip was used as the potential electrode (positive and/or negative). Greater surface area (about 4 mm) of the current source and sink electrodes was exposed to the host material to generate large current. The potential electrodes were always maintained as a point electrode (exposure of just the tip of the copper wire).

For the pole-pole electrode configuration, the current sink electrode (B) was placed at the bottom of the tank and the potential sink electrode (N) was placed at the other diagonal of the tank's bottom.

Various models (e.g. aluminium cylinder with different diameters and shapes, drilled rock cores made of different materials and impurities etc) were used as the target which was immerged in the ordinary tap water (host material). Because of a wide range of electrical resistivity (conductivity) which can occur in nature, these target models were used to represent in quantitative way the simplest geological situations.

The target was orientated on the x-y plane perpendicular to the profile. For example, in the bipole-bipole configuration the two electrodes A and M were on the x-y plane at the positions: x-coordinate = 25 cm, y-coordinate = 30 cm from the edge of the tank. Similarly, the electrodes B and N were at: x-coordinate = 35 cm, y-coordinate = 30 cm.

The tank was filled with ordinary tap water and a resistive rock (diameter 5 cm) was suspended from the string at a depth of 20 cm below the surface of water. The true resistivity of tap water was 7 ohm.m and that of the rock cylinder was unknown. The experiment was conducted with the bipole-bipole AM-BN configuration. The observed data were obtained at 1cm spacing sampling with 5 cm separation of current source electrode (A) and current sink electrode (B) over the depth range 10 cm to 35 cm for each electrode A, and positive potential electrode (M) positions (Fig. 1). The distance between electrode (B) and negative potential electrode (N) was 5 cm. In total there were 21 x 21 = 441 data points for imaging.

The first experiment was carried out with the rock cylinder positioned approximately in the middle of the tank. The apparent resistivity of the rock cylinder was selected similar to the apparent resistivity of aquifer. The rock cylinder was placed perpendicular to the array profiling. Tap water was used to simulate the confining layer surrounding the aquifer. The model dimensions were scaled to the field situation of aquifer at the field site in South Australia. The imaging of aquifer (whose strike direction was horizontal to the crosshole survey) was performed using bipole-bipole AM-BN configuration by two vertical rods which were simulated as two observation wells in a crosshole survey.

Field observations

The site used for field observations is located approximately 20 km northwest of the Adelaide Central Business District on the Northern Adelaide Plains. Beneath the Adelaide Plains, the Port Willunga Formation is characterised by a thick subsurface section (>100 m) which is laterally extensive across the sub-basin. This unit is hydrostratigraphically divided into an upper sandy limestone facies (T1 aquifer) and a lower, sometimes dense blocky limestone (T2 aquifer) separated by the Munno Para Clay Member which forms a laterally extensive aquifer across the sub-basin. This study deals with the Tertiary sediments of the Port Willunga Formation of the Adelaide sub-basin that forms part of the much larger St. Vincent Basin.

The water bearing units within the Tertiary sequence also include the Dry Creek/Hallett Cove Sand which lies above the Port Willunga Formation. Because of the existence of a semi-confining bed, the T1 aquifer is further divided into sub-aquifers: the T1(a) aquifer which comprises the Hallett Cove/Dry Creek Sand and the T1(b) aquifer composed of the sandy limestone facies of the Upper Port Willunga Formation.

The observation wells penetrated the T2 aquifer and were drilled to a total depth of 212 m using rotary mud drilling. Cutting samples were collected at 3 m intervals over the entire penetrated depth. The wells were developed by airlifting at a rate of 10 to 15 litres per second. It required three days of airlifting before the well stopped producing sand. The well was left to recover. Completion of the wells was carried out using 203 mm ID Fibre Reinforced Plastic (FRP) casing with the casing shoe set at a depth of 100 m. The casing was then pressure cemented to surface whilst the remaining section of the well (100 m to 212 m that encompasses the entire thickness of the T2 aquifer at this site) was left as an open hole completion.

After preliminary development by airlifting, a water sample was obtained from the open hole section in the T2 aquifer and the electrical conductivity of 2910 μS/cm inferred a total dissolved solids (TDS) content of 1600 milligram per litre. The analysis of sample from the T2 aquifer indicated a uniform porosity of 0.35. The chemical analyses of the aquifer material showed the dominant mineral to be calcite with quartz sub-dominant. The transmissivity of the T2 aquifer was 310 $m^3\ day^{-1}\ m^{-1}$.

An electrical resistivity field experiment was conducted using borehole-to-borehole tomography before injection of fresh water into T2 aquifer (Lower Port Willunga Formation). Two mobile electrodes spaced 15 m apart were lowered inside the two observation wells. The distances of the four electrodes were measured from the surface. The upper two

electrodes (positive and negative electrodes) were placed at a depth of 114 m. All four electrodes (current source, current sink, positive potential, and negative potential) were moved with an array spacing of 1 m using the crosshole scanning method to the depth of 160 m.

RESULTS OF EXPERIMENTS/ OBSERVATIONS

Fig. 2 gives the results of the laboratory experiment. It shows that the shape of the cylinder is distorted due to the limited illumination (coverage of the object was confined to the maximum angle range from -60° to 60°). The position of the cylinder has been shifted up owing to the errors in electrode locations. The result gives a reasonable image of the resistive target. It shows that the bipole-bipole electrode configuration is indeed suitable for crosshole resistivity imaging of aquifers.

Fig. 3 gives the result for the electrical resistivity tomography experiment between two observation wells for the T2 aquifer. Fig. 3a shows the presence and distribution of apparent resistivity values in the T2 aquifer (Lower Port Willunga Formation) and its confining layers (Munno Para Clay and Ruwarrung Member) before injection of fresh water into the aquifer. The starting model used for the geophysical inversion is shown in Fig. 3b.

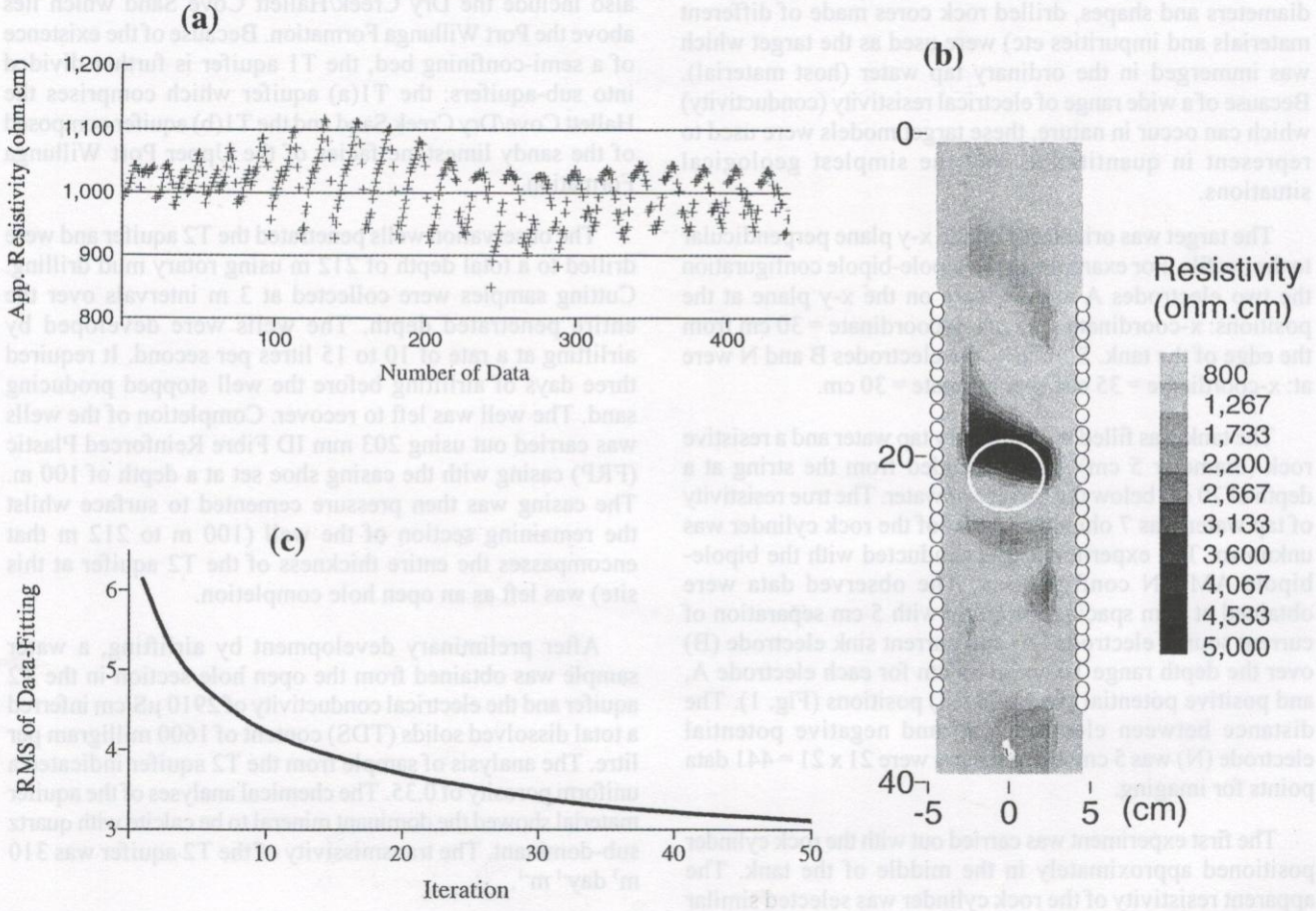

Fig. 2: Physical modelling data and electrical resistivity imaging result with the crosshole bipole-bipole AM-BN configuration for a resistive rock cylinder: (a) apparent resistivity, (b) imaging result, and (c) inversion convergence curve. In (b) the circle indicates the location of the rock cylinder (cross-section).

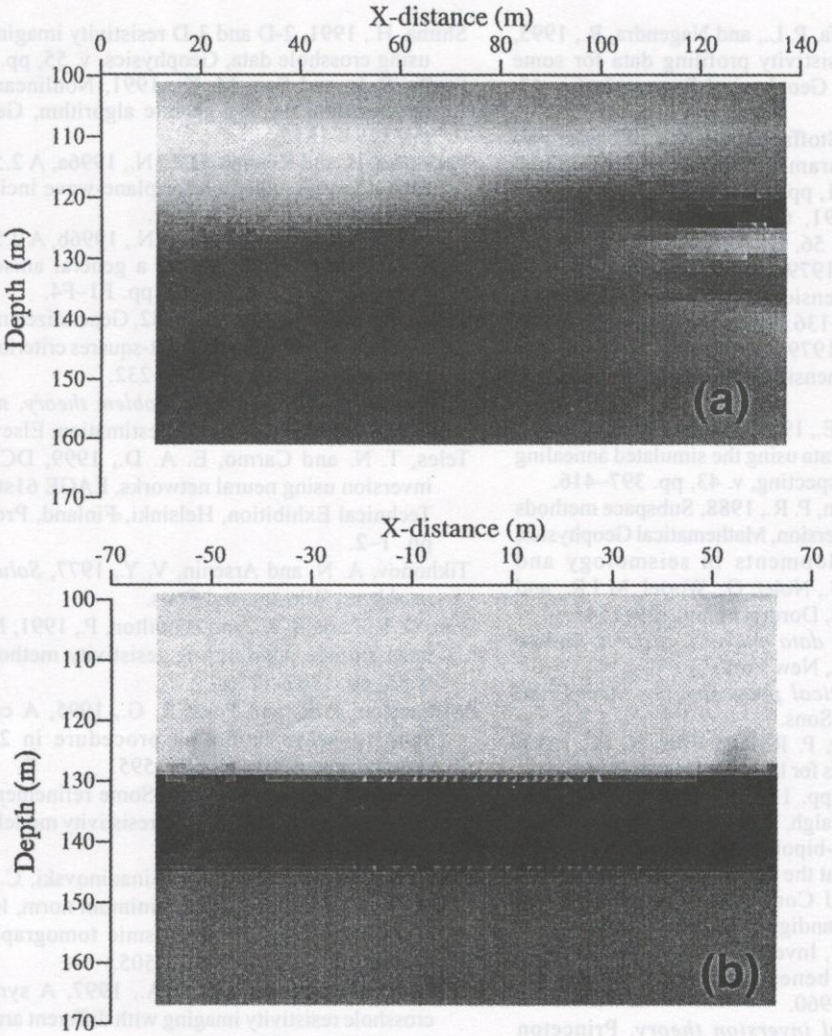

Fig. 3: Field experiments of electrical resistivity imaging result with the crosshole bipole-bipole AM-BN configuration performed to observation wells for the T2 aquifer (Lower Port Willunga Formation): (a) starting model used for the inversion algorithms and (b) imaging of T2 aquifer and confining layers (Munno Para Clay and Ruwarrung Member).

CONCLUSIONS

A finite element method (FEM) scheme, which utilises the 2.5-D Helmholtz equation to compute the Green's function, is found both flexible and efficient for 2.5-D forward resistivity modelling. The geophysical inversion method applied is found robust for inversion of DC resistivity data.

Results of the physical model experiments and field experiments conducted to investigate and examine the effectiveness of the borehole-to-borehole aquifer imaging with bipole-bipole AM-BN electrode array prove that electrical resistivity tomography method is effective for imaging aquifers.

ACKNOWLEDGEMENTS

The author acknowledges the Royal Nepal Academy of Science and Technology (RONAST), Nepal, for financial support extended to prepare and present this paper at the International Symposium on "Engineering Geology, Hydrogeology and Natural Disasters with Emphasis on Asia", 28-30 September, 1999, Kathmandu, Nepal.

REFERENCES

Cao, S. and Greenhalgh, S. A., 1997, 2.5-D acoustic wave modeling in the wave number-frequency domain, Exploration Geophysics, v. 28, pp. 11–15.

Chunduru, R., Sen, M. K., Stoffa, P. L., and Nagendra, R., 1995, Non-linear inversion of resistivity profiling data for some regular geometrical bodies, Geophysical Prospecting, v. 43, pp. 979–1003.

Chunduru, R., Sen, M. K., and Stoffa, P. L., 1996, 2-D resistivity inversion using spline parameterization and simulated annealing, Geophysics, v. 61, pp. 151–161.

Daily, W. and Owen, E., 1991, Cross-borehole resistivity tomography, Geophysics, v. 56, pp. 1228–1235.

Dey, A. and Morrison, H. F., 1979a, Resistivity modeling for arbitrarily shaped two-dimensional structure, Geophysical Prospecting, v. 27, pp. 106–136.

Dey, A. and Morrison, H. F., 1979b, Resistivity modeling for arbitrarily shaped three-dimensional structure, Geophysics, v. 44, pp. 753–780.

Dittmer, J. K. and Szymenski, J. E., 1995, The stochastic inversion of magnetics and resistivity data using the simulated annealing algorithm, Geophysical Prospecting, v. 43, pp. 397–416.

Kennett, B. L. N. and Williamson, P. R., 1988, Subspace methods for large-scale non-linear inversion, Mathematical Geophysics, a survey of recent developments in seismology and geodynamics, eds Vlaar, N.J., Nolet, G., Wortel, M.J.R., and Cloetingh, S.A.L., D. Reidel, Dordrecht, pp. 139–154.

Menke, W., 1984, *Geophysical data analysis: discrete inverse theory*, Academic Press, Inc., New York.

Minoux, M., 1986, *Mathematical programming theory and algorithms*, John Wiley and Sons.

Oldenburg, D. W., McGillicray, P. R., and Ellis, R. G., 1993, Generalised subspace methods for large-scale inverse problems, Geophys. Jour. Int., v. 114, pp. 12–20.

Pant, D. R., Bing, Z., and Greenhalgh, S. A., 1999, Physical model studies of inversion of bipole-bipole resistivity data for aquifer imaging, A paper presented at the Association of Exploration Geophysicists 25th Annual Convention and Seminar on Exploration Geophysics, Chandigarh, India, Abstract.

Park, S. K. and Van, G. P., 1991, Inversion of pole-pole data for 3-D resistivity structure beneath array of electrodes, Geophysics, v. 56, pp. 951–960.

Parker, R., 1994, *Geophysical inversion theory*, Princeton University Press, Princeton, New Jersey.

Queralt, J. P. and Marcuello, A., 1991, 2-D resistivity modeling: an approach to arrays parallel to the strike direction, Geophysics, v. 56, pp. 941–950.

Scales, J. A. and Smith, M. L., 1994, *Introductory geophysical inverse theory*, Smizdat Press Golden, White River Junction.

Shima, H., 1991, 2-D and 3-D resistivity imaging reconstruction using crosshole data, Geophysics, v. 55, pp. 682–694.

Stoffa, P. L. and Sen, M. K., 1991, Nonlinear multiparameter optimization using a genetic algorithm, Geophysics, v. 56, pp. 1794–1810.

Takenaka, H. and Kennett, B. L. N., 1996a, A 2.5-D time-domain elastodynamic equation for plane-wave incidence, Geophys. Jour. Int., v. 124, pp. F5–F9.

Takenaka, H. and Kennett, B. L. N., 1996b, A 2.5-D time-domain elastodynamic equation for a general anisotropic medium, Geophys. Jour. Int., v. 127, pp. F1–F4.

Tarantola, A. and Vallette, B., 1982, Generalized non-linear inverse problem solved using the least-squares criterion, Rev. Geophys. Space Phys., v. 20, pp. 219–232.

Tarantola, A., 1987, *Inverse problem theory*, methods for data fitting and model parameter estimation, Elsevier.

Teles, T. N. and Carmo, E. A. D., 1999, DC resistivity data inversion using neural networks, EAGE 61st Conference and Technical Exhibition, Helsinki, Finland, Proceedings PO97, pp. 1–2.

Tikhonov, A. N. and Arsenin, V. Y., 1977, *Solution of ill-posed problems*, Winston and Sons.

Van, G. P., Park, S. K., and Hamilton, P., 1991, Monitoring leaks from storage ponds using resistivity methods, Geophysics, v. 56, pp. 1267–1270.

Williamson, P. R. and Pratt, R. G., 1995, A critical review of acoustic wave modeling procedure in 2.5 dimensions, Geophysics, v. 60, pp. 591–595.

Zhao, S. and Yedlin, M., 1996, Some refinements on the finite-difference method for 3-D dc resistivity modeling, Geophysics, v. 61, pp. 1301–1307.

Zhou, B., Greenhalgh, S., and Sinadinovski, C., 1992, Iterative algorithm for the damped minimum norm, least squares and constrained problem in seismic tomography, Exploration Geophysics, v. 23, pp. 497–505.

Zhou, B. and Greenhalgh, S. A., 1997, A synthetic study on crosshole resistivity imaging with different arrays, Exploration Geophysics, v. 28, pp. 1–5.

Zhou, B. and Greenhalgh, S. A., 1998, A damping method for 2.5-D Green's function for arbitrary acoustic media, Geophys. Jour. Int., v. 133, pp. 111–120.

Zienkiewicz, 1971, *The finite element method in engineering science*, McGraw-Hill Book Company, Inc.